



Letter

Robust Range Ambiguous Deceptive Target Suppression Based on Covariance Matrix Reconstruction

Zhuang Xie ¹, Jiahua Zhu ^{2,*}, Chongyi Fan ¹, Xiaotao Huang ¹ and Jian Wang ¹

¹ College of Electronic Science and Technology, National University of Defense Technology, Changsha 410073, China; xiezhuang18@nudt.edu.cn (Z.X.); chongyifan@nudt.edu.cn (C.F.); xthuang@nudt.edu.cn (X.H.); jianwang_uwb@nudt.edu.cn (J.W.)

² College of Meteorology and Oceanography, National University of Defense Technology, Changsha 410073, China

* Correspondence: zhujiahua1019@nudt.edu.cn

Abstract: When the deceptive targets are in the ambiguous range bin but are received at the same range gate with the desired target by the array, the traditional multiple-input multiple-output (MIMO) radar is not able to discriminate between them. Based on the unique range-dependent beampattern of the frequency diverse array (FDA)-MIMO radar, we propose a novel robust mainlobe deceptive target suppression method based on covariance matrix reconstruction to form nulls at the frequency points of the transmit–receive domain where deceptive targets are located. First, the proposed method collects the deceptive targets and noise information in the transmit–receive frequency domain to reconstruct the jammer-noise covariance matrix (JNCM). Then, the covariance matrix of the desired target is constructed in the desired target region, which is assumed to already be known. The transmit–receive steering vector (SV) of the desired target is estimated to be the dominant eigenvector of the desired target covariance matrix. Finally, the weighting vector of the receive beamformer is calculated by combining the reconstructed JNCM and the estimated desired target SV. By implementing the weighting vector at the receiving end, the deceptive targets can be effectively suppressed. The simulation results demonstrate that the proposed method is robust to SV mismatches and provides a signal-to-jamming-plus-noise ratio (SJNR) output that is close to the optimal.

Keywords: FDA-MIMO; transmit–receive frequency; receive beamforming; steering vector; deceptive target suppression



Citation: Xie, Z.; Zhu, J.; Fan, C.; Huang, X.; Wang, J. Robust Range Ambiguous Deceptive Target Suppression Based on Covariance Matrix Reconstruction. *Remote Sens.* **2021**, *13*, 2346. <https://doi.org/10.3390/rs13122346>

Academic Editors: Andrzej Staczny and Paolo Addesso

Received: 1 December 2020

Accepted: 8 June 2021

Published: 16 June 2021

Publisher's Note: MDPI stays neutral with regard to jurisdictional claims in published maps and institutional affiliations.



Copyright: © 2021 by the authors. Licensee MDPI, Basel, Switzerland. This article is an open access article distributed under the terms and conditions of the Creative Commons Attribution (CC BY) license (<https://creativecommons.org/licenses/by/4.0/>).

1. Introduction

The Frequency diverse array (FDA) is a new type of radar array that was proposed by Antonik [1,2] and is quite different from the traditional phased array. It has unique range-dependent beampattern characteristics as it introduces frequency increments among the transmitted signals [3]. The FDA has an extra degree of freedom in the range domain which provides new opportunities for radar target detection and tracking. However, the range-dependent beampattern of the basic FDA radar varies with time, which imposes great limitations on its application [4]. In order to effectively utilize the FDA's degree of freedom in the distance dimension, many methods have been proposed to overcome the limitation of time-varying effects. A time-varying frequency increment strategy for FDA was derived in [5], which uses a time-dependent frequency offset among the antennas to obtain the time-independent beampattern, but this continuous frequency change is difficult to implement in practice. The pulsed-FDA was proposed by [6] together with several constraints to obtain the quasi-static beampattern. However, it was proven that the derived constraint is too rigorous. Two schemes of the frequency offset were proposed by Yao et al to deal with the time-varying problem for short-range scenarios and multitarget scenarios [7,8]. The multicarrier architecture was implemented by Wang et al in the FDA to

obtain a time-invariant beampattern [9]. However, the above time-invariant beamforming method only allows the peak of the beam to stay at that distance for a short period of time, and it cannot focus the frequency-controlled array transmitting beam at a given distance [10].

The multiple-input multiple-output (MIMO) radar performs better than the phased array in terms of target localization, tracking, and detection due to its extended aperture [11–13], while the FDA has a better ranging performance due to its unique degree of freedom in the range dimension. By introducing the frequency diversity to the MIMO radar, the FDA-MIMO radar was proposed, and it received attention due to its considerable potential [14,15]. In the FDA-MIMO radar, a group orthogonal waveforms is transmitted with a small carrier frequency increment among the antennas. With beamforming technology at the receiving end, a range-angle-dependent beampattern is generated [16]. Different from the traditional phased array radar, the unique beampattern of FDA-MIMO radar brings additional freedom degree in the range dimension which can be further explored in suppressing range-dependent jammers.

The repeating jammer with the digital radio frequency memory technique is able to intercept and analyze transmitted radar waveforms. The jammer replicates the radar waveforms and re-transmits the waveform with additional Doppler modulation and time delay. By controlling the additional time delay and Doppler frequency modulation, the repeating jammer is capable of placing the generated targets at any doppler and range bin. The traditional phased array is not able to recognize the deceptive targets generated by the repeating jammer, especially when the deceptive targets are in the mainlobe [17], while the FDA-MIMO radar with the extra degree of freedom in the range domain can suppress the mainlobe deceptive targets. Xu et al. utilized the FDA-MIMO radar to distinguish real and deceptive targets in the range-angle domain and the range-dependent beampattern of FDA-MIMO to suppress mainlobe deceptive targets [18,19]. Deep nulls are formed precisely in the range-angle plane to effectively suppress the deceptive targets, but the derived signal model is just a special case and is not suitable for more complicated scenarios [20].

In terms of mainlobe deceptive targets suppression, there are various methods proposed trying to find the difference between the true target and the deceptive target in other domains such as time, frequency or polarization domain [21–23]. However, these methods are ineffective for the case when the deceptive target echo is received by the array in the same range gate with the true target. In this paper, we aim to suppress the range ambiguous mainlobe deceptive targets which are received at the same range gate with the desired target at the array. The contributions of this paper are as follows.

- We propose a novel robust mainlobe deceptive target suppression method based on covariance matrix reconstruction to suppress the deceptive targets in the mainlobe. First, the proposed method reconstructs the deceptive targets and noise covariance matrix with the Capon power spectrum over the complementary region of the desired target region (DTR). Therefore, the reconstructed covariance matrix only collects information about deceptive targets and noise. Then, similarly, the covariance matrix of the desired target including the steering vector (SV) information of the desired target is constructed through integrating the Capon power spectrum over the DTR. The transmit–receive SV of the desired target is estimated as the dominant eigenvector of the desired target covariance matrix. Finally, the weighting vector of the receive beamformer is calculated by combining the reconstructed jammer-noise covariance matrix (JNCM) and the estimated desired target SV.

The deceptive targets considered here are special interferences which cannot be discriminated in the spatial or range domain, which makes the extraction of the desired target signal very hard. By applying the proposed robust beamforming algorithm based on the FDA-MIMO radar, not only can the interfering components be effectively suppressed, but also the mainlobe can be adjusted towards the desired target robustly. Therefore, the proposed method is a pre-processing technique; the data with other undesired components eliminated can be used for parameter estimation or other applications. The simulation

results demonstrate that the proposed method has an excellent level of performance and is robust to the desired SV mismatch. It provides a signal-to-jamming-plus-noise ratio (SJNR) output that is close to optimal.

2. FDA-MIMO Signal Model

We consider an omnidirectional uniform linear FDA consisting of M array elements which acts as both a transmitting and a receiving array. The carrier frequencies f_m of transmitting signals differs from element to element, i.e., $f_m = f_0 + (m - 1)\Delta f$, $m = 1, 2, \dots, M$. f_0 is the reference frequency and Δf is the frequency increment between adjacent elements [16]. The transmitted signal for the m th array element is

$$s_m(t) = \phi_m(t) \cdot \exp(j2\pi f_m t) \tag{1}$$

where $\phi_m(t)$ is the complex waveform envelope for the m th transmitting element. It is assumed that these envelopes are orthogonal with each other and can be separated through matched filtering. In the far-field case, for a target located in the direction θ_T and at a distance r_T from the reference element (the first element), the time delay of the signal radiated by the m th element and received by the n th element is given as

$$\tau_{m,n} = \tau_0 - \tau_{Tm} - \tau_{Rn} = \frac{2r_T}{c} - \frac{d(m - 1)\sin(\theta_T)}{c} - \frac{d(n - 1)\sin(\theta_T)}{c} \tag{2}$$

where d is the inter-element spacing. $\tau_0 \triangleq \frac{2r_T}{c}$ is the common time delay term, $\tau_{Tm} \triangleq \frac{d(m-1)\sin(\theta_T)}{c}$ and $\tau_{Rn} \triangleq \frac{d(n-1)\sin(\theta_T)}{c}$ are the time delays caused by the transmitting and receiving array structures, respectively. Therefore, the signal received by the n th element can be written as

$$\begin{aligned} y_n(t) &= \sum_{m=1}^M \delta_T \cdot \phi_m(t - \tau_{m,n}) \cdot \exp(j2\pi f_m(t - \tau_{m,n})) \\ &= \sum_{m=1}^M \delta_T \cdot \phi_m(t - \tau_0 + \tau_{Tm} + \tau_{Rn}) \cdot \exp(j2\pi f_m(t - \tau_0 + \tau_{Tm} + \tau_{Rn})) \end{aligned} \tag{3}$$

where δ_T is the complex reflect coefficient of the target.

With the waveform assumed to be in the narrowband, i.e., $\phi_m(t - \tau_{m,n}) \approx \phi_m(t - \tau_0)$, after matched filtering with the reference signal $\phi_m(t) \cdot e^{j2\pi f_m t}$, the signal radiated by the m th element and received by the n th element can be separated and written in snapshot form [16] as

$$\begin{aligned} y_{m,n} &\approx \delta_T \cdot \exp\left\{j2\pi\left(f \frac{d(m - 1)\sin(\theta_T)}{c} - 2\Delta f \frac{(m - 1)r_T}{c}\right)\right\} \exp\left\{j2\pi f \frac{d(n - 1)\sin(\theta_T)}{c}\right\} \\ &= \delta_T \cdot \exp\{j2\pi(m - 1)f_T\} \exp\{j2\pi(n - 1)f_R\} \end{aligned} \tag{4}$$

In the derivation above, $f_T \triangleq f \frac{d\sin(\theta_T)}{c} - 2\Delta f \frac{r_T}{c}$ is the transmitting frequency and $f_R \triangleq f \frac{d\sin(\theta_T)}{c}$ is the frequency received by the target. Therefore, after matched filtering, the received data can be expressed in snapshot form as

$$\mathbf{y}_T = \delta_T \cdot \mathbf{v} = \delta_T \cdot \mathbf{a}_T(f_T) \otimes \mathbf{a}_R(f_R) \tag{5}$$

where $\mathbf{v}(f_T, f_R) \triangleq \mathbf{a}_T(f_T) \otimes \mathbf{a}_R(f_R)$ is the transmit–receive SV. The $M \times 1$ transmit SV $\mathbf{a}_T(f_T)$ and receive SV $\mathbf{a}_R(f_R)$ have the following expressions:

$$\begin{aligned} \mathbf{a}_T(f_T) &= [1, \exp(j2\pi f_T), \dots, \exp(j2\pi(M - 1)f_T)]^T \\ &= \left[1, \exp(j2\pi\left(f \frac{d\sin(\theta_T)}{c} - 2\Delta f \frac{r_T}{c}\right)), \dots, \exp(j2\pi(M - 1)\left(f \frac{d\sin(\theta_T)}{c} - 2\Delta f \frac{r_T}{c}\right))\right]^T \end{aligned} \tag{6}$$

$$\begin{aligned} \mathbf{a}_R(f_R) &= [1, \exp(j2\pi f_R), \dots, \exp(j2\pi(M-1)f_R)]^T \\ &= \left[1, \exp(j2\pi(f \frac{d \sin(\theta_T)}{c})), \dots, \exp(j2\pi(M-1)(f \frac{d \sin(\theta_T)}{c})) \right]^T \end{aligned} \quad (7)$$

3. Model of Range Ambiguous Deceptive Jammer

The deceptive target generator is able to intercept and replicate the radar waveform. It re-transmits the captured waveform with an additional time delay and Doppler modulation to generate unreal targets at any range bin, thereby deceiving the receiver. For an interceptor in the direction θ_{itc} and range r_{itc} , the intercepted waveform is

$$x(t) = \sum_{m=1}^M \phi_m(t - \tau_{itc}) \cdot \exp(j2\pi f_m(t - \tau_{itc})) \quad (8)$$

where $\tau_{itc} = \frac{r_{itc}}{c}$ is the real time delay of the intercepted signal transmitted by the reference element of the array. Since the deceptive jamming in the different direction with desired target can be mitigated through spatial filtering, we consider a worst case, i.e., the interceptor is placed in the same direction as the desired target. In the following content, we assume that $\theta_{itc} = \theta_T$. Since the jammer needs time to analyze and replicate the waveform, the deceptive signals are assumed to fall behind at least one pulse after the pulse of interception. In this paper, we mainly focus on the case that the deceptive jamming is placed in the same direction as the desired target and in the ambiguity range bin. The deceptive jamming is received by the array in the same range gate with the desired target and cannot be filtered in spatial or range domain. The existing method dealing with this situation is to change the pulse repetitive frequency (PRF) to distinguish this kind of interference [24]. Suppose the pulse repetitive time (PRT) of the radar is T , the actual time delay of the deceptive signal received by the reference element is $\tau_{dec,k}$, where k is the ambiguity number, $k = 1, 2, \dots, K$. For the deceptive targets placed in the ambiguous same range bin with the desired target, $\tau_{dec,k}$ has the following form:

$$\tau_{dec,k} = kT + \tau_0 \quad k = 1, \dots, K \quad (9)$$

where K is the maximum number of ambiguities. As shown in Figure 1a, the deceptive targets return to the receiver at the same range gate as the desired target. It should be noted that the phase difference among the receiving elements only result from the receiving structure. Therefore, in terms of the time delay of the deceptive signal received by the n th element, it has the form $\tau_{dec,k} - \tau_{Rn}$, where $\tau_{Rn} \triangleq \frac{d(n-1)\sin(\theta_T)}{c}$ is the same as before. According to the time delay term, for the deceptive target placed in the k th range ambiguous bin, the deceptive signal received by n th element of the array is expressed as

$$y_{d,n}(t) = \sum_{m=1}^M \delta_{dec,k} \cdot \phi_m(t - \tau_{dec,k} + \tau_{Rn}) \cdot \exp(j2\pi f_m(t - \tau_{dec,k} + \tau_{Rn})) \quad (10)$$

where $\delta_{dec,k}$ is the Doppler modulation. It can be clearly observed that the involved deceptive targets have a significant influence on the desired target detection. Since the deceptive jamming signals are usually strong in terms of power, the desired target may be submerged. Furthermore, as the deceptive targets are at the same direction and range gate as the desired target, the traditional MIMO radar cannot effectively suppress the deceptive targets from the angle domain. The FDA-MIMO radar, on the other hand, is capable of forming a range-dependent beam pattern because of the extra degree of freedom created by the introduction of frequency diversity among the antennas. Since the deceptive targets and the desired targets in fact have different time delays, they can be separated in the transmit–receive frequency domain. In the FDA-MIMO radar, the targets are separated in

the transmit frequency domain. The frequency interval between adjacent targets is ΔfT , as shown in Figure 1b. By forming nulls at the frequency points of the deceptive targets, we can effectively suppress them by utilizing the FDA-MIMO radar.

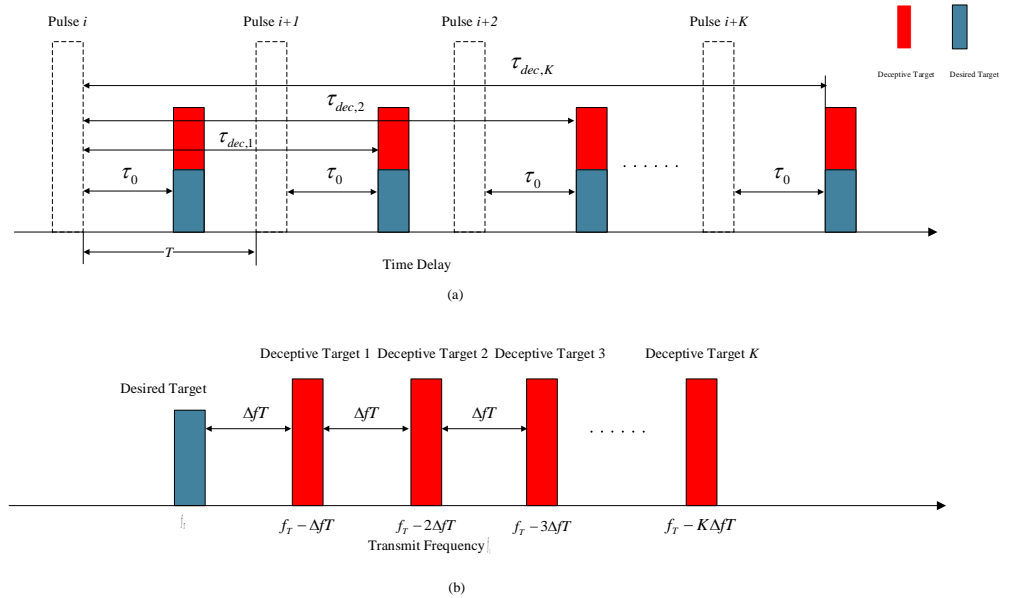


Figure 1. Illustration of range ambiguous deceptive targets in FDA-MIMO radar. (a) Range ambiguous deceptive targets in the time domain, (b) the desired target and deceptive targets in the transmit frequency domain.

In this case, when the deceptive targets exist, after matched filtering, the received data are expressed in vector form as

$$\begin{aligned}
 \mathbf{y} &= \mathbf{y}_T + \mathbf{y}_{dec} + \mathbf{n} \\
 &= \delta_T \cdot \mathbf{a}_T(f_T) \otimes \mathbf{a}_R(f_R) + \sum_{k=1}^K \delta_{dec,k} \cdot \mathbf{a}_T(f_T + \Delta f(k-1)T) \otimes \mathbf{a}_R(f_R) + \mathbf{n} \\
 &= \delta_T \cdot \mathbf{v}(f_T, f_R) + \sum_{k=1}^K \delta_{dec,k} \cdot \mathbf{v}(f_T + \Delta f(k-1)T, f_R) + \mathbf{n}
 \end{aligned} \tag{11}$$

where \mathbf{n} is the $M^2 \times 1$ complex noise vector, which is considered to be white Gaussian with variance σ_n^2 . As introduced before, $\mathbf{v}(f_T, f_R)$ is the transmit–receive SV at frequency point (f_T, f_R) . $\mathbf{y}_{dec} = \sum_{k=1}^K \delta_{dec,k} \cdot \mathbf{a}_T(f_T + \Delta f(k-1)T) \otimes \mathbf{a}_R(f_R) = \sum_{k=1}^K \delta_{dec,k} \cdot \mathbf{v}(f_T + \Delta f(k-1)T, f_R)$ is the deceptive target component of the received snapshot. Since the deceptive targets are different from the desired target in the transmitting frequency domain, we can utilize the beamforming technique to form nulls in the transmitting frequency domain. The weighting vector of the Minimum Variance Distortionless Response (MVDR) beamformer is described as

$$\mathbf{w} = \frac{\mathbf{R}_{j+n}^{-1} \mathbf{v}(f_T, f_R)}{\mathbf{v}^H(f_T, f_R) \mathbf{R}_{j+n}^{-1} \mathbf{v}(f_T, f_R)} \tag{12}$$

where $\mathbf{R}_{j+n} \triangleq \sum_{k=1}^K \mathbf{v}(f_T + \Delta f(k-1)T, f_R) \mathbf{v}^H(f_T + \Delta f(k-1)T, f_R) + \sigma_n^2 \mathbf{I}$ is the JNCM. Since the precise JNCM is unavailable in practice, it is usually replaced by the sample covariance matrix (SCM) which utilizes sample snapshots to approximate \mathbf{R}_{j+n} [25,26]. Assuming there are L pulses per CPI, then the SCM is calculated as

$$\hat{\mathbf{R}} = \frac{1}{L} \sum_{l=1}^L \mathbf{y}_l^H \mathbf{y}_l \tag{13}$$

where \mathbf{y}_l is the l th snapshot, and L represents the number of snapshots. By replacing the JNCM with the SCM, we actually obtain the sample matrix inversion (SMI) beamformer as

$$\mathbf{w} = \frac{\hat{\mathbf{R}}^{-1} \mathbf{v}(f_T, f_R)}{\mathbf{v}^H(f_T, f_R) \hat{\mathbf{R}}^{-1} \mathbf{v}(f_T, f_R)} \tag{14}$$

4. Robust Ambiguous Range Deceptive Target Suppression Based on Covariance Matrix Reconstruction

It should be pointed out that the performance of the SMI beamformer will suffer severe deterioration at a high signal-to-noise ratio (SNR) due to the existence of the desired signal [25]. The desired signal is regarded as interference at high SNRs and is suppressed by the noise subspace. In the following text, we introduce the proposed method which can achieve significant SINR improvement by mitigating the covariance matrix error arising from the existence of the desired signal. To remove the desired signal component from the SCM, we reconstruct the JNCM based on the transmit–receive frequency 2D Capon spectrum. By collecting interference information in the region where the desired signal is excluded, we obtain the reconstructed JNCM.

Suppose that the desired signal is located in DTR Θ of the transmit–receive frequency domain which excludes the deceptive targets, as shown in Figure 2. The DTR Θ is assumed to already be known since it can be determined by low-resolution finding methods. The widths of the regions are marked as Θ_T and Θ_R , respectively.

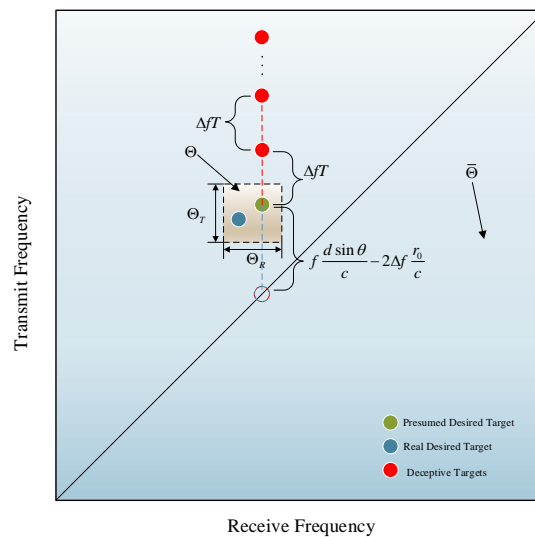


Figure 2. Illustration of DTR in the transmit–receive domain.

The Capon spectrum is a high resolution spectrum with no sidelobe. It reflects the power distribution over the transmit–receive domain. Across the whole frequency plane, the power of different frequency points can be indicated by the Capon power spectrum. By combining the estimated power and SV, we can reconstruct the JNCM. To begin with, the transmit–receive frequency 2D Capon spectrum is expressed as

$$P_{\text{capon}}(f_t, f_r) = \frac{1}{[\mathbf{a}_T(f_t) \otimes \mathbf{a}_R(f_r)]^H \hat{\mathbf{R}}^{-1} [\mathbf{a}_T(f_t) \otimes \mathbf{a}_R(f_r)]} \tag{15}$$

where $P_{\text{Capon}}(f_t, f_r)$ reflects the power strength of the received data at frequency point (f_t, f_r) .

We denote the complementary region of Θ as $\bar{\Theta}$. As shown in Figure 2, $\bar{\Theta}$ in the transmit–receive frequency domain only contains frequency points where the deceptive targets are located. Therefore, by integrating the Capon spectrum over the $\bar{\Theta}$, the JNCM is reconstructed as

$$\begin{aligned}\hat{\mathbf{R}}_{i+n} &= \iint_{\bar{\Theta}} P_{\text{capon}}(f_t, f_r) \mathbf{v}(f_t, f_r) \mathbf{v}^H(f_t, f_r) df_t df_r \\ &= \iint_{\bar{\Theta}} \frac{[\mathbf{a}_T(f_t) \otimes \mathbf{a}_R(f_r)] \cdot [\mathbf{a}_T(f_t) \otimes \mathbf{a}_R(f_r)]^H}{[\mathbf{a}_T(f_t) \otimes \mathbf{a}_R(f_r)]^H \hat{\mathbf{R}}^{-1} [\mathbf{a}_T(f_t) \otimes \mathbf{a}_R(f_r)]} df_t df_r\end{aligned}\quad (16)$$

It can be clearly observed that the reconstructed JNCM includes the deceptive targets transmit–receive SV information and excludes the desired signal transmit–receive SV information. For computation, the whole frequency domain is discretized into $Q = Q_t \times Q_r$ points, including Q_t points in the transmit frequency domain with frequency interval Δf_t and Q_r points in the receive frequency domain with frequency interval Δf_r . Suppose there are $Q_{\bar{\Theta}}$ points in the complement region $\bar{\Theta}$ and each single point corresponds to a transmit–receive frequency, i.e., $\bar{\Theta}$ in the transmit–receive frequency domain contains $Q_{\bar{\Theta}}$ frequency points as $(f_{t,1}, f_{r,1}), (f_{t,2}, f_{r,2}), \dots, (f_{t,Q_{\bar{\Theta}}}, f_{r,Q_{\bar{\Theta}}})$. Then, the summation process is substituted for the integral process as

$$\begin{aligned}\hat{\mathbf{R}}_{i+n} &= \sum_{i=1}^{Q_{\bar{\Theta}}} P_{\text{capon}}(f_{t,i}, f_{r,i}) \mathbf{v}(f_{t,i}, f_{r,i}) \mathbf{v}^H(f_{t,i}, f_{r,i}) \\ &= \sum_{i=1}^{Q_{\bar{\Theta}}} \frac{[\mathbf{a}_T(f_{t,i}) \otimes \mathbf{a}_R(f_{r,i})] \cdot [\mathbf{a}_T(f_{t,i}) \otimes \mathbf{a}_R(f_{r,i})]^H}{[\mathbf{a}_T(f_{t,i}) \otimes \mathbf{a}_R(f_{r,i})]^H \mathbf{R}^{-1} [\mathbf{a}_T(f_{t,i}) \otimes \mathbf{a}_R(f_{r,i})]}\end{aligned}\quad (17)$$

For the desired signals, there are evidently mismatches in the accurate SV and the presumed SV. To enhance the accuracy of the desired target transmit–receive SV, we propose a new approach to estimate the transmit–receive SV of the desired target which involves no convex optimization operation. The covariance matrix reconstruction concept is applied again to collect the information of the desired target in the DTR first. We denote the frequency points located in the DTR as $(f_{t,Q_{\bar{\Theta}}+1}, f_{r,Q_{\bar{\Theta}}+1}), (f_{t,Q_{\bar{\Theta}}+2}, f_{r,Q_{\bar{\Theta}}+2}), \dots, (f_{t,Q}, f_{r,Q})$. Then, the desired signal covariance matrix is constructed as

$$\begin{aligned}\hat{\mathbf{R}}_d &= \sum_{i=Q_{\bar{\Theta}}+1}^Q P_{\text{capon}}(f_{t,i}, f_{r,i}) \mathbf{v}(f_{t,i}, f_{r,i}) \mathbf{v}^H(f_{t,i}, f_{r,i}) \\ &= \sum_{i=Q_{\bar{\Theta}}+1}^Q \frac{[\mathbf{a}_T(f_{t,i}) \otimes \mathbf{a}_R(f_{r,i})] \cdot [\mathbf{a}_T(f_{t,i}) \otimes \mathbf{a}_R(f_{r,i})]^H}{[\mathbf{a}_T(f_{t,i}) \otimes \mathbf{a}_R(f_{r,i})]^H \mathbf{R}^{-1} [\mathbf{a}_T(f_{t,i}) \otimes \mathbf{a}_R(f_{r,i})]}\end{aligned}\quad (18)$$

since the expression above collects information in the desired region, it only contains the desired signal information. The desired signal SV can be estimated as

$$\hat{\mathbf{v}}(f_T, f_R) = P[\hat{\mathbf{R}}_d] \quad (19)$$

where $P[\cdot]$ stands for the principle eigenvector operator. It should be noted that the performance of the beamformer will not be affected by multiplying the desired target SV with a nonzero scalar. It can be clearly observed from the above derivations that the proposed approach collects the information in the DTR and estimates the desired SV as the principle eigenvector of the constructed covariance matrix, which corresponds to the desired SV. The proposed desired SV estimating approach only needs to know the DTR and thereby is robust to desired SV mismatches.

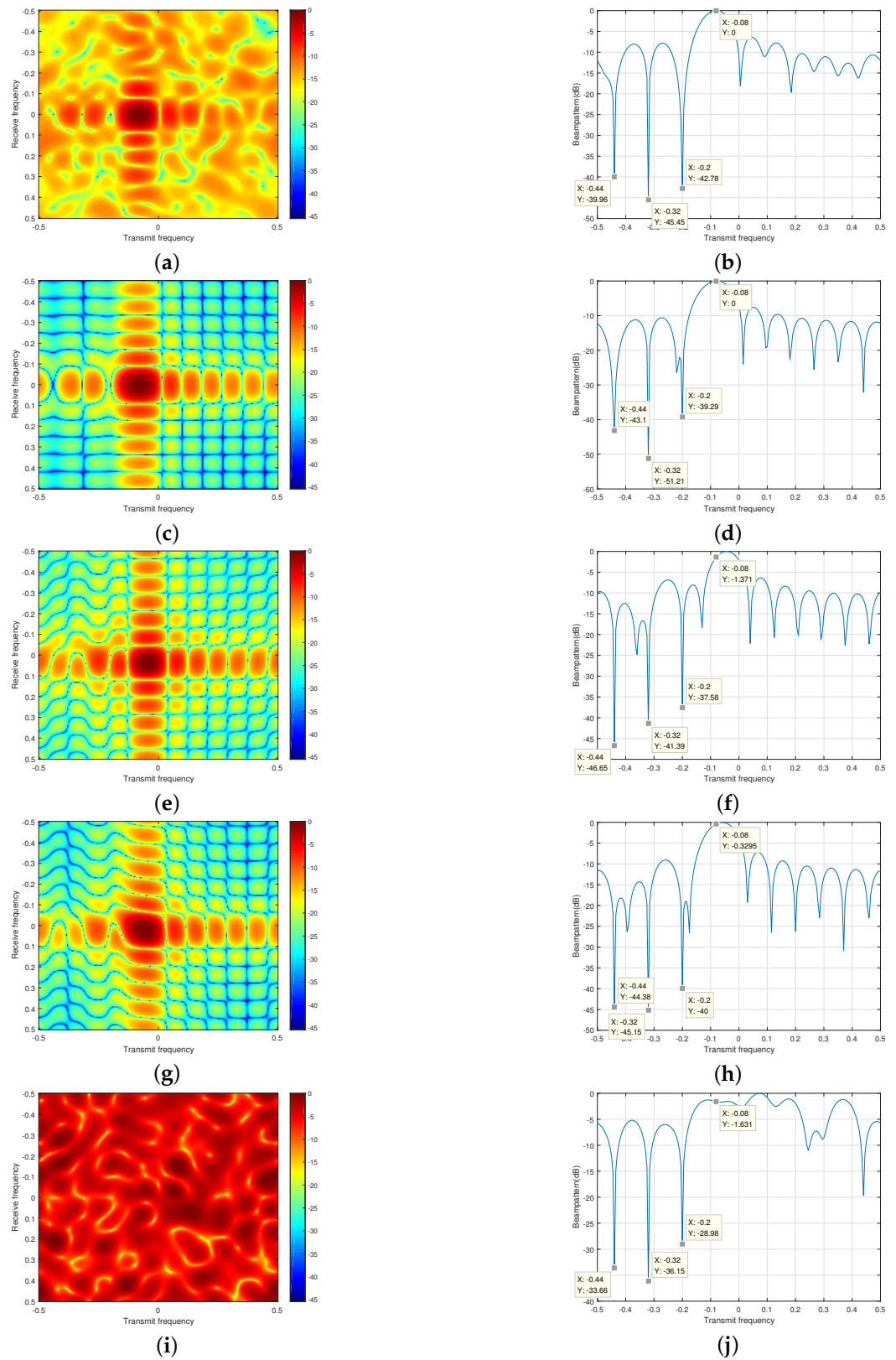


Figure 3. Beam-patterns of different methods in transmit–receive domain and cross section at $f_r = 0$ (SNR = -30 dB). (a,b) Optimal, (c,d) proposed method (with SV estimation process), (e,f) LSMI-MVDR, (g,h) proposed method (without SV estimation process), (i,j) Eigenspace method.

Based on the reconstructed JNCM and the estimated SV of the desired target, the proposed beamformer is obtained by

$$\mathbf{w} = \frac{\hat{\mathbf{R}}_{I+n}^{-1} \hat{\mathbf{v}}(f_T, f_R)}{\hat{\mathbf{v}}(f_T, f_R)^H \hat{\mathbf{R}}_{I+n}^{-1} \hat{\mathbf{v}}(f_T, f_R)} \quad (20)$$

The main complexity of the proposed method lies in the covariance matrix reconstruction process and the eigendecomposition of the estimated desired signal covariance matrix $\hat{\mathbf{R}}_d$. It should be noted that the dimension of transmit–receive steering vector is $M^2 \times 1$ since the array size is M . In terms of the covariance matrix reconstruction process, it consists of two parts: the reconstruction of JNCM and the construction of desired target covariance matrix. Therefore, the computational complexity is $\mathcal{O}((M^2)^2 \cdot (Q_{\Theta} + Q - Q_{\Theta}))$ in terms of the number of flops. The complexity of the eigendecomposition of the desired target covariance matrix is $\mathcal{O}((M^2)^3)$. Therefore, the computational complexity of the proposed method is generally $\mathcal{O}\{\max(M^6, M^4Q)\}$.

5. Simulation

In this section, simulation results are provided to validate the good performance of the FDA-MIMO radar in terms of suppression of deceptive targets in the ambiguity range bin. The general simulation parameters are shown in Table 1.

Table 1. Simulation parameters.

Parameter	Value	Parameter	Value
Size of the array	10	Noise power	0 dB
Reference carrier frequency	1.5 GHz	Real target angle	0°
Pulses per CPI	400	Assumed target angle	4°
Frequency increment	2 KHz	Target range	6 km
PRF	33 KHz	JNR	30 dB

The radar considered here is used for low-altitude air-to-ground scenario, the radar is set on a helicopter or a drone. The proposed method eliminates the mainlobe jamming to make the data better for the following use. Without any loss of generality, the element spacing of the FDA array is set to be half of the minimum transmitted wavelength among the antennas as

$$\begin{aligned} d &= \min \left\{ \frac{\lambda_1}{2}, \frac{\lambda_2}{2}, \dots, \frac{\lambda_M}{2} \right\} \\ &= \min \left\{ \frac{1}{2} \cdot \frac{c}{f_1}, \frac{1}{2} \cdot \frac{c}{f_2}, \dots, \frac{1}{2} \cdot \frac{c}{f_M} \right\} \\ &= \frac{1}{2} \cdot \frac{c}{f_0 + (M-1)\Delta f} \\ &= 0.1 \end{aligned} \quad (21)$$

In these examples, the corresponding transmit–receive frequency point for the desired target is $(-0.008, 0)$. In all examples, the ambiguity number considered is 3, i.e., the furthest deceptive target is $3\Delta f T c$ away from the desired target. The transmit–receive frequencies of the deceptive targets are $(-0.44, 0)$, $(-0.32, 0)$ and $(-0.2, 0)$, respectively. In the proposed method, we assume that the width of the desired target region is 0.04 and, therefore, the region is $\Theta_T = [-0.012, -0.004]$ and $\Theta_R = [-0.004, 0.004]$. The region is discretized into $M = 100$ points. To better illustrate the superiority of the proposed method, the results of proposed method (without the SV estimation process), diagonal loading sample matrix inversion (LSMI) MVDR, the eigenspace methods as well as optimal are added for comparison. The loading factor is chosen to be 10 dB over the noise power for the LSMI-MVDR method and the deceptive target number is assumed to be accurately

known for the eigenspace method. The weighting vector of optimal is calculated with the accurately known \mathbf{R}_{j+n} and desired SV $\mathbf{v}(f_T, f_R)$ as

$$\mathbf{w} = \frac{\mathbf{R}_{j+n}^{-1} \mathbf{v}(f_T, f_R)}{\mathbf{v}^H(f_T, f_R) \mathbf{R}_{j+n}^{-1} \mathbf{v}(f_T, f_R)} \quad (22)$$

For all examples, 500 Monte Carlo trials are performed to obtain the results.

5.1. Example 1

In this section, we draw the beampattern of the beamformers to examine the deceptive target suppression ability of the proposed method in the FDA-MIMO array. Figure 3 presents the transmit–receive frequency beampatterns with a fixed SNR of -30 dB. Figure 3a,c,e,g,i illustrate the optimal transmit–receive beampatterns as well as those of the proposed method (with the SV estimation process), LSMI-MVDR, the proposed method (without the SV estimation process) and the eigenspace method, respectively. It is shown in the figure that there are deep nulls in the frequency points corresponding to the deceptive targets in all beampatterns except for that of the eigenspace method, which means that the deceptive targets involved in the received data can be suppressed effectively. Though the beamformers provide nulls deeper than -30 dB at the three frequency points, it can be seen that, in the eigenspace method, the mainlobes are distorted and the desired target is suppressed. For better illustration, we draw the cross section beampattern of different methods at $f_r = 0$, as shown in Figure 3b,d,f,h,j. Cursors are marked in the cross section beampatterns. The mainlobes of the LSMI-MVDR, proposed method (without the SV estimation process) as well as the eigenspace method are mismatched and the maximum peak is not pointed towards the desired target $(-0.08, 0)$, while the mainlobe of the proposed method (with the SV estimation process) is steered accurately towards $(-0.08, 0)$.

Figure 4 presents the beampatterns with a fixed SNR of 0 dB. Figure 4e,f draw the beampattern of the LSMI-MVDR method. From the drawn figures, it can be clearly observed that, as the input SNR becomes higher, the existence of the desired signal in the SCM degrades the performance of the LSMI-MVDR beamformer. The nulls at the three deceptive frequency points are shallow and the sidelobes are high. The mismatch of the desired SV is more obvious. The desired target is also suppressed by the LSMI-MVDR beamformer. Figure 4c,d show the detect detection ability of the proposed method. Compared with the result shown in Figure 3, it is clear that the proposed method is insensitive to the SNR strength due to the removal of the desired signal in the covariance matrix. Maintenance of the null shape at the frequency points can be seen clearly in Figure 4d, and the suppression ability of the proposed method is still close to optimal. The mainlobe is accurately pointed towards the transmitting frequency of the desired target.

As the SNR becomes closer to 30 dB, Figure 5 shows the beampattern results with a significant difference. From Figure 5e,f, it can be observed that the LSMI-MVDR is ineffective in terms of providing a satisfactory output SINR. The self-nulling effect becomes very obvious: the desired signal is regarded as a deceptive interference and is suppressed along with the deceptive ones. The mainlobe is completely mismatched. This indicates that, at high SNRs, the SCM cannot be used as a replacement of JNCM. The desired signal component in the SCM significantly degrades the output SINR performance. We can see that in Figure 5e,f the sidelobe of the LSMI-MVDR method is high and the suppression of deceptive targets is ineffective. Figure 5c,d present the beampattern of the proposed method. It has a good detection performance and is capable of suppressing the deceptive targets to -35 dB lower. The proposed method removes the desired signal component by reconstructing the JNCM and therefore forms more shaper nulls. Figure 5g,h illustrate the performance of the proposed method (without the SV estimation process), which is satisfactory but has a deviation from the proposed method. It can be seen that the mainlobe is slightly mismatched. This deviation arises from the desired target SV errors, while,

in contrast, the proposed method is robust against the desired SV mismatch and obtains a significant performance improvement.

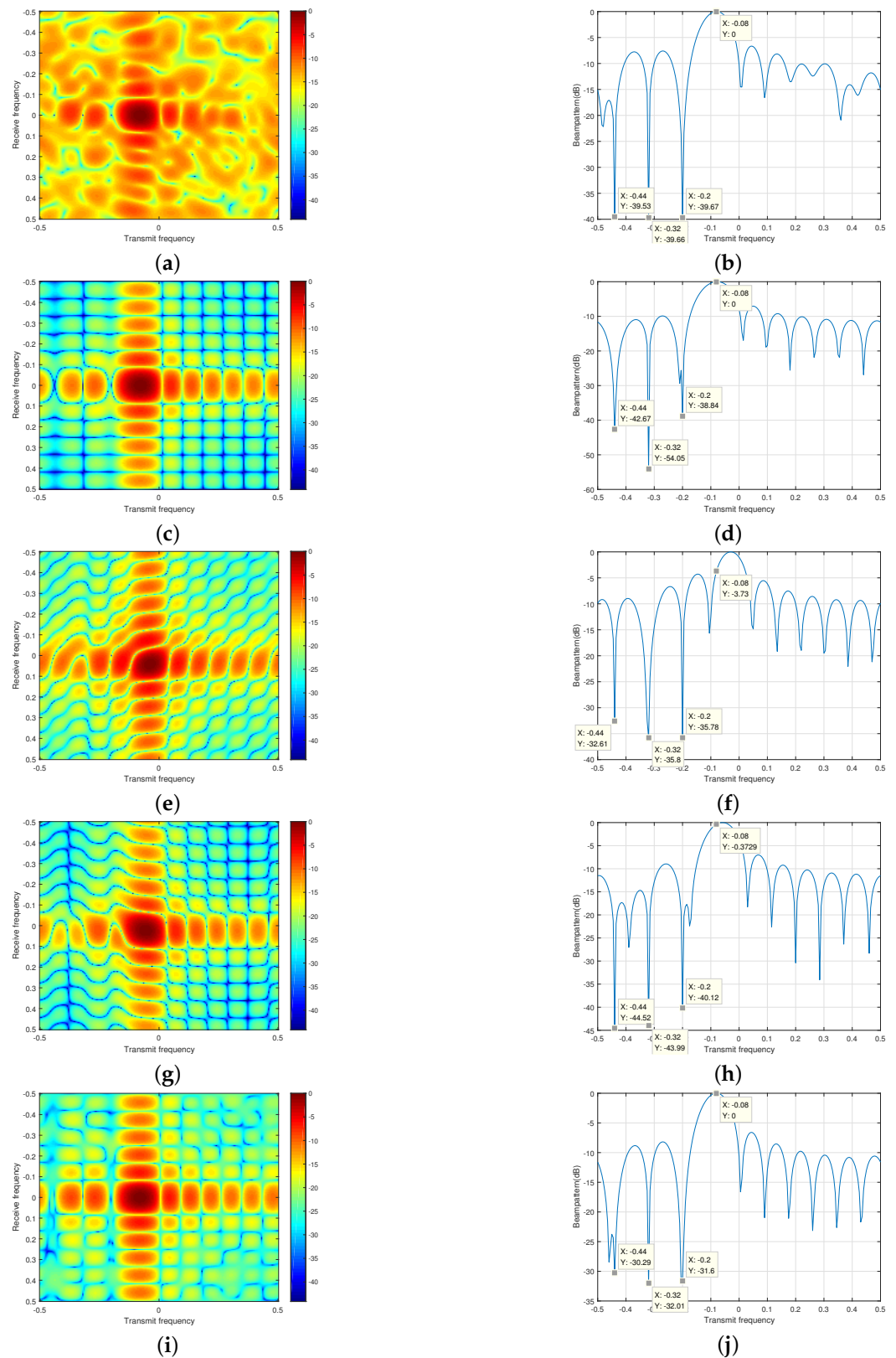


Figure 4. Beam-patterns of different methods in the transmit–receive domain and cross section at $f_T = 0$ (SNR = 0 dB). (a,b) Optimal, (c,d) proposed method (with the steering vector (SV) estimation process), (e,f) LSMI-MVDR, (g,h) proposed method (without the SV estimation process), (i,j) Eigenspace method.

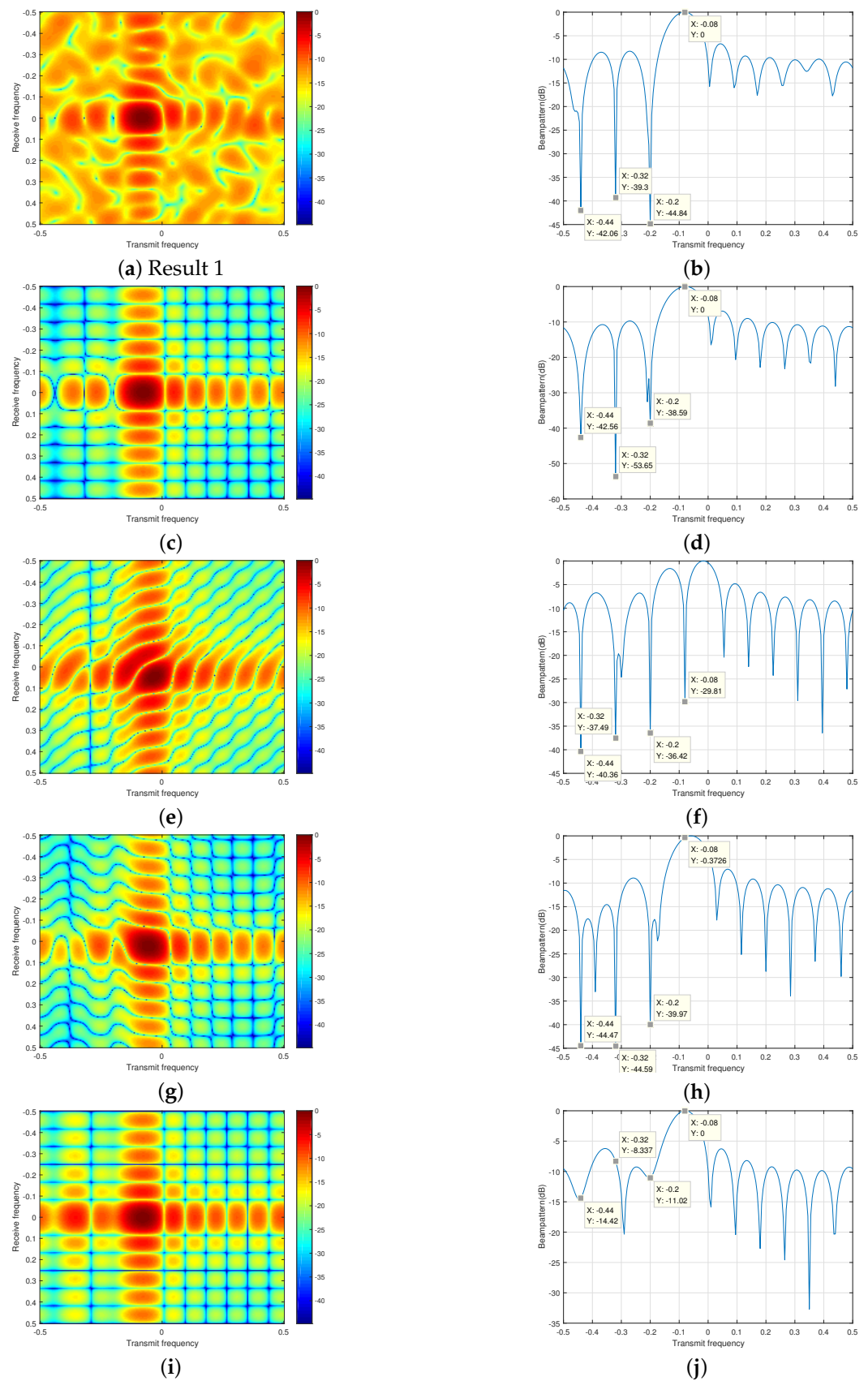


Figure 5. Beam-patterns of different methods in the transmit–receive domain and cross section at $f_r = 0$ (SNR = 30 dB). (a,b) Optimal, (c,d) proposed method (with the SV estimation process), (e,f) LSMI-MVDR, (g,h) proposed method (without the SV estimation process), (i,j) Eigenspace method.

5.2. Example 2

The output SJNR curves versus the input SNR are used in this section to examine the target detection ability of the FDA-MIMO radar using different methods. The SJNR is calculated by

$$SJNR = \frac{\mathbf{w}^H \mathbf{R}_d \mathbf{w}}{\mathbf{w}^H \mathbf{R}_{j+n} \mathbf{w}} \quad (23)$$

where \mathbf{w} is the weighting vector of different methods and \mathbf{R}_d is the theoretical covariance matrix of the desired signal. Figure 6 shows the output SJNR and its deviations from the optimal SJNR versus the input SNR. It can be noticed that both LSMI-MVDR and the proposed method provide high output SJNR values at low SNRs. As the SNR becomes higher, the performance of the LSMI-MVDR method drops sharply and the deviation from the optimal value increases due to the existence of the desired signal in the SCM. The performance of the eigenspace method is moderate. It is able to show a satisfactory performance with a high SJNR output at SNRs from -20 to 0 dB. However, the performance is poor at other SNRs. The proposed method shows excellent performance in all SNRs. The output SJNR of the proposed method stays very close to optimal at all SNRs and is insensitive to the SNR strength. It is worth noting that the proposed method with the SV estimation process is able to achieve a 4 dB improvement compared with the proposed method without the SV estimation process under circumstances when there are errors in prior knowledge about the desired target SV. There is a deviation between the assumed and real mainlobe pointing directions, which is consistent with example 1. This indicates that the proposed method is robust to the absence of prior knowledge about the desired SV.

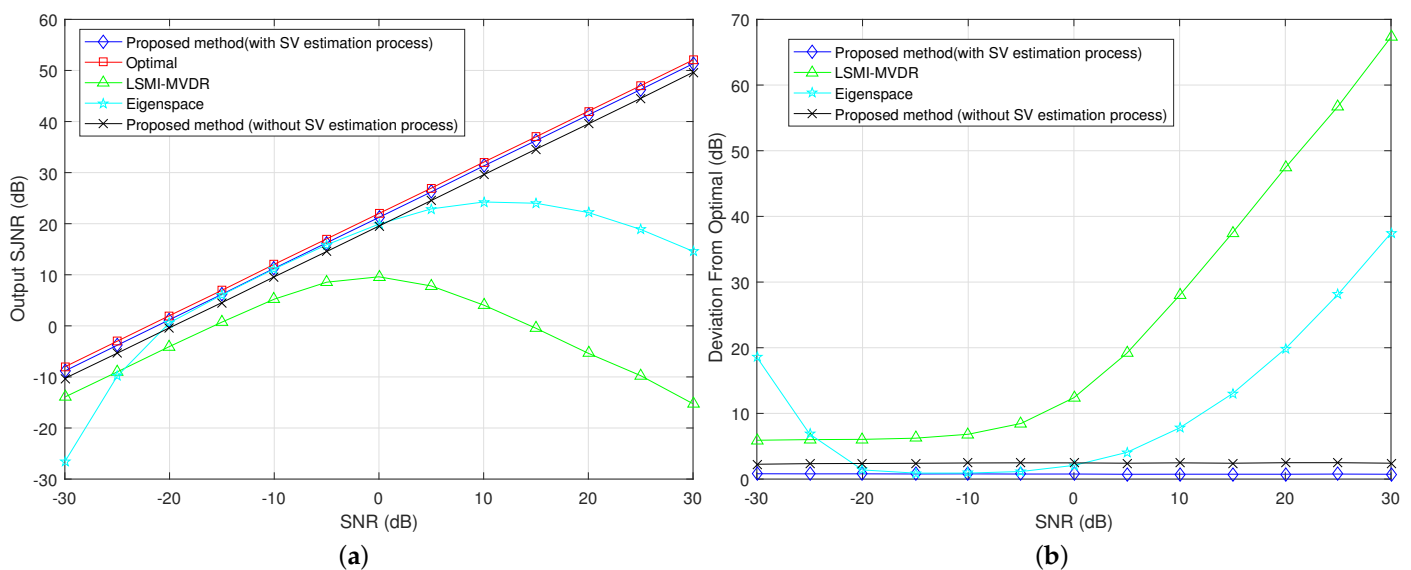


Figure 6. SJNR output performance of different methods. (a) Output SJNR versus input signal-to-noise ratio (SNR) (b) output SJNR deviation from the optimal value.

6. Conclusions

In this paper, we proposed a novel robust mainlobe range ambiguous deceptive target suppression method which can be implemented in the FDA-MIMO radar. The range-dependent beampattern of the FDA-MIMO radar can be utilized to suppress the ambiguous range deceptive targets, which cannot be achieved by a phased array radar. The proposed method uses the beamforming technique to form nulls at the frequency points where deceptive targets are located in the transmit–receive frequency domain. The covariance matrix reconstruction concept is applied to exclude the desired target component in the received samples and estimate the SV of the desired target. The simulation results show that the proposed method attains a satisfactory SJNR output that is very close to the

optimal value and is robust against desired target SV mismatch. It should be noted that the proposed model is not applicable for the moving target objects. In this paper, we actually focus on the non-moving target. In terms of the moving target object, the corresponding processing method will be listed as a further extension work.

Author Contributions: Conceptualization, Z.X. and J.Z.; methodology, Z.X.; software, Z.X.; validation, Z.X., J.Z. and C.F.; writing—original draft preparation, Z.X., J.Z. and J.W.; writing—review and editing, J.Z., C.F., J.W., and X.H.; supervision, J.W., X.H. All authors have read and agree to the published version of the manuscript.

Funding: This research received no external funding.

Conflicts of Interest: The authors declare no conflict of interest.

References

1. Antonik, P.; Wicks, M.C.; Griffiths, H.D.; Baker, C.J. Range-dependent beamforming using element level waveform diversity. In Proceedings of the 2006 International Waveform Diversity Design Conference, Lihue, HI, USA, 22–27 January 2006; pp. 1–6.
2. Antonik, P.; Wicks, M.C.; Griffiths, H.D.; Baker, C.J. Multi-mission multi-mode waveform diversity. In Proceedings of the 2006 IEEE Conference on Radar, Verona, NY, USA, 24–27 April 2006; p. 3
3. Wang, W. Frequency Diverse Array Antenna: New Opportunities. *IEEE Antennas Propag. Mag.* **2015**, *57*, 145–152. [[CrossRef](#)]
4. Secmen, M.; Demir, S.; Hizal, A.; Eker, T. Frequency Diverse Array Antenna with Periodic Time Modulated Pattern in Range and Angle. In Proceedings of the 2007 IEEE Radar Conference, Waltham, MA, USA, 17–20 April 2007; pp. 427–430.
5. Khan, W.; Qureshi, I.M. Frequency Diverse Array Radar with Time-Dependent Frequency Offset. *IEEE Antennas Wirel. Propag. Lett.* **2014**, *13*, 758–761. [[CrossRef](#)]
6. Xu, Y.; Shi, X.; Xu, J.; Li, P. Range-Angle-Dependent Beamforming of Pulsed Frequency Diverse Array. *IEEE Trans. Antennas Propag.* **2015**, *63*, 3262–3267. [[CrossRef](#)]
7. Yao, A.; Wu, W.; Fang, D. Frequency Diverse Array Antenna Using Time-Modulated Optimized Frequency Offset to Obtain Time-Invariant Spatial Fine Focusing Beampattern. *IEEE Trans. Antennas Propag.* **2016**, *64*, 4434–4446. [[CrossRef](#)]
8. Yao, A.; Rocca, P.; Wu, W.; Massa, A.; Fang, D. Synthesis of Time-Modulated Frequency Diverse Arrays for Short-Range Multi-Focusing. *IEEE J. Sel. Top. Signal Process.* **2017**, *11*, 282–294. [[CrossRef](#)]
9. Wang, Y.; Li, W.; Huang, G.; Li, J. Time-Invariant Range-Angle-Dependent Beampattern Synthesis for FDA Radar Targets Tracking. *IEEE Antennas Wirel. Propag. Lett.* **2017**, *16*, 2375–2379. [[CrossRef](#)]
10. Chen, B.; Chen, X.; Huang, Y.; Guan, J. Transmit Beampattern Synthesis for the FDA Radar. *IEEE Antennas Wirel. Propag. Lett.* **2018**, *17*, 98–101. [[CrossRef](#)]
11. Fishler, E.; Haimovich, A.; Blum, R.; Chizhik, D.; Cimini, L.; Valenzuela, R. MIMO radar: An idea whose time has come. In Proceedings of the 2004 IEEE Radar Conference (IEEE Cat. No.04CH37509), Philadelphia, PA, USA, 29 April 2004; pp. 71–78.
12. Davis, M.S.; Showman, G.A.; Lanterman, A.D. Coherent MIMO radar: The phased array and orthogonal waveforms. *IEEE Aerosp. Electron. Syst. Mag.* **2014**, *29*, 76–91. [[CrossRef](#)]
13. Liu, W.; Wang, Y.; Liu, J.; Xie, W.; Chen, H.; Gu, W. Adaptive detection without training data in colocated MIMO radar. *IEEE Trans. Aerosp. Electron. Syst.* **2015**, *51*, 2469–2479. [[CrossRef](#)]
14. Wen, C.; Tao, M.; Peng, J.; Wu, J.; Wang, T. Clutter Suppression for Airborne FDA-MIMO Radar Using Multi-Waveform Adaptive Processing and Auxiliary Channel STAP. *Signal Process.* **2019**, *154*, 280–293. [[CrossRef](#)]
15. Wang, C.; Xu, J.; Liao, G.; Xu, X.; Zhang, Y. A Range Ambiguity Resolution Approach for High-Resolution and Wide-Swath SAR Imaging Using Frequency Diverse Array. *IEEE J. Sel. Top. Signal Process.* **2017**, *11*, 336–346. [[CrossRef](#)]
16. Sammartino, P.F.; Baker, C.J.; Griffiths, H.D. Frequency Diverse MIMO Techniques for Radar. *IEEE Trans. Aerosp. Electron. Syst.* **2013**, *49*, 201–222. [[CrossRef](#)]
17. Vorobyov, S.A.; Gershman, A.B.; Luo, Z.-Q. Robust adaptive beamforming using worst-case performance optimization: A solution to the signal mismatch problem. *IEEE Trans. Signal Process.* **2003**, *51*, 313–324. [[CrossRef](#)]
18. Xu, J.; Liao, G.; Zhu, S.; So, H.C. Deceptive jamming suppression with frequency diverse MIMO radar. *Signal Process.* **2015**, *113*, 9–17. [[CrossRef](#)]
19. Lan, L.; Liao, G.; Xu, J.; Zhang, Y.; Fioranelli, F. Suppression Approach to Main-Beam Deceptive Jamming in FDA-MIMO Radar Using Nonhomogeneous Sample Detection. *IEEE Access* **2018**, *6*, 34582–34597. [[CrossRef](#)]
20. Shi, J.; Liu, X.; Yang, Y.; Sun, J.; Wang, N. Comments on “Deceptive jamming suppression with frequency diverse MIMO radar”. *Signal Process.* **2018**, *158*, 1–3. [[CrossRef](#)]
21. Akhtar, J.; Olsen, K.E. Frequency agility radar with overlapping pulses and sparse reconstruction. In Proceedings of the 2018 IEEE Radar Conference (RadarConf18), Oklahoma City, OK, USA, 23–27 April 2018; pp. 0061–0066.
22. Xiang, Z.; Chen, B.; Yang, M. Transmitter/receiver polarisation optimisation based on oblique projection filtering for mainlobe interference suppression in polarimetric multiple-input-multiple-output radar. *IET Radar Sonar Navig.* **2018**, *12*, 137–144. [[CrossRef](#)]

23. Ding, L.; Li, R.; Wang, Y.; Dai, L.; Chen, F. Discrimination and identification between mainlobe repeater jamming and target echo by basis pursuit. *IET Radar Sonar Navig.* **2017**, *11*, 11–20. [[CrossRef](#)]
24. Li, J.; Stoica, P. *MIMO Radar Signal Processing*; John Wiley & Sons: Hoboken, NJ, USA, 2008.
25. Gu, Y.; Leshem, A. Robust adaptive beamforming based on interference covariance matrix reconstruction and steering vector estimation. *IEEE Trans. Signal Process.* **2012**, *60*, 3881–3885.
26. Zheng, Z.; Yang, T.; Wang, W.Q.; So, H.C. Robust adaptive beamforming via simplified interference power estimation. *IEEE Trans. Aerosp. Electron Syst.* **2019**, *55*, 3139–3152. [[CrossRef](#)]